Title

Outbreak of densovirus with high mortality in a commercial mealworm (Tenebrio molitor) farm: A molecular, bright-field, and electron microscopic characterization.

Journal

Veterinary Pathology, 60(5)

Authors

Armién, Aníbal
Polon, Robert
Rejmanek, Daniel
et al.

Publication Date

2023-09-01

DOI

10.1177/03009858231180488

Peer reviewed

Veterinary Pathology
2023, Vol. 60(5) 689–703

DOI: 10.1177/03009858231180488
journals.sagepub.com/home/vet


Outbreak of densovirus with high mortality in a commercial mealworm (*Tenebrio molitor*) farm: A molecular, bright-field, and electron microscopic characterization

Aníbal G. Armién[1], Robert Polon[1], Daniel Rejmanek[1], Robert B. Moeller[1], and Beate M. Crossley[1]

Abstract

Mealworms are one of the most economically important insects in large-scale production for human and animal nutrition. Densoviruses are highly pathogenic for invertebrates and exhibit an extraordinary level of diversity which rivals that of their hosts. Molecular, clinical, histological, and electron microscopic characterization of novel densovirus infections is of utmost economic and ecological importance. Here, we describe an outbreak of densovirus with high mortality in a commercial mealworm (*Tenebrio molitor*) farm. Clinical signs included inability to prehend food, asymmetric locomotion evolving to nonambulation, dehydration, dark discoloration, and death. Upon gross examination, infected mealworms displayed underdevelopment, dark discoloration, larvae body curvature, and organ/tissue softness. Histologically, there was massive epithelial cell death, and cytomegaly and karyomegaly with intranuclear inclusion (InI) bodies in the epidermis, pharynx, esophagus, rectum, tracheae, and tracheoles. Ultrastructurally, these InIs represented a densovirus replication and assembly complex composed of virus particles ranging from 23.79 to 26.99 nm in diameter, as detected on transmission electron microscopy. Whole-genome sequencing identified a 5579-nucleotide-long densovirus containing 5 open reading frames. A phylogenetic analysis of the mealworm densovirus showed it to be closely related to several bird- and bat-associated densoviruses, sharing 97% to 98% identity. Meanwhile, the nucleotide similarity to a mosquito, cockroach, and cricket densovirus was 55%, 52%, and 41%, respectively. As this is the first described whole-genome characterization of a mealworm densovirus, we propose the name *Tenebrio molitor* densovirus (*Tm*DNV). In contrast to polytropic densoviruses, this *Tm*DNV is epitheliotropic, primarily affecting cuticle-producing cells.

Keywords

densovirus, electron microscopy, epitheliotropic virus, histopathology, mealworm, mortality, *Parvoviridae*, *Tenebrio* molitor, virus assembly, virus replication

As the human population continues to grow, so will its demand for protein.[34] In the Western portion of the world, livestock farming covers the vast majority of protein production; however, the insect farming industry is quickly expanding, producing protein-rich products with a relatively low ecological footprint.[15] Insects are poikilotherms, meaning they do not rely on metabolic energy to regulate their body temperature. This allows them to allocate more energy toward growth, resulting in a higher feed conversion efficiency.[27,41]

Yellow mealworms (YMWs, *Tenebrio molitor*) are one of the most economically important insects in large-scale production.[15] They are used as pet food and livestock feed with increasing commonality due to their high protein, fat, and polyunsaturated fatty acid contents.[15,21] YMWs have recently been considered ideal for human nutrition, offering a more cost- and energy-efficient alternative protein source to livestock and aquaculture.[15] Not only have they been proven to thrive on diets of agricultural byproducts,[41] YMWs have also been shown to degrade polystyrene, a polymer found in plastics that is highly resistant to environmental degradation.[40,45]

Increased use of insects as a protein source for either humans or livestock poses the challenge of novel infectious disease outbreaks via pathogenic infection by any number of microorganisms (ie, viruses, bacteria, fungi, protists, nematodes). The high population density of insect farming exacerbates the spread of disease in these populations and increases the likelihood of epidemics and zoonotic transmission.[2,12]

[1]University of California, Davis, Davis, CA

Corresponding Author:
Aníbal G. Armién, California Animal Health & Food Safety Lab System, University of California, Davis, 620 W. Health Sciences Drive, Davis, CA 95616, USA.
Email: agarmien@ucdavis.edu

Densoviruses are autonomous, nonenveloped, paraspherical DNA viruses that are 23 to 28 nm in diameter with icosahedral symmetry and contain 5 kb, single-stranded, linear DNA genomes.[8] They belong to the subfamily *Densovirinae* within the *Parvoviridae* family.[43] *Densovirinae* contains 1 unassigned species and 5 genera, which are *Ambidensovirus, Brevidensovirus, Hepandensovirus, Iteradensovirus*, and *Penstyldensovirus*.[8] Comprising more than 20 viral species, most members of the subfamily *Densovirinae* are highly pathogenic for invertebrates. Currently, densoviruses are known to infect insects from 6 orders (*Blattodea, Diptera, Hemiptera, Hymenoptera, Lepidoptera*, and *Orthoptera*), decapod crustaceans (shrimp and crayfish), and echinoderms (sea stars).[8,38] In addition, densoviruses have been devastating to commercially produced invertebrate populations, such as the cricket,[24,36] silkworm,[23] and shrimp.[11,33] Densovirus infections were initially referred to as "densonucleosis," a term used to indicate the large, dense, and homogeneous appearance of infected nuclei (nuclear inclusions) of greater wax moth (*Galleria mellonella*) larvae due to replication of a small virus (later to be designated as a densovirus).[8,23] A significant number of densoviruses are polytropic with a variable host range, while other densovirus infections are host- and organ-specific.[38] The high pathogenicity of densovirus to pests, especially mosquitos, favors its use as a biological control agent,[22] although the long-term impact of viral spillover among nontarget native insect populations remains unknown.[26]

Insects represent the most biodiverse group of animals on Earth,[37] with more than 2000 species being consumed by humans worldwide.[18] Unlike viruses affecting vertebrates/mammals, densoviruses are as diverse as their invertebrate hosts.[38] This is reflected in the wide range of biological behaviors displayed among different densovirus species.[8] Still, little is known about viruses affecting insects, including those used for food and feed.[12] Characterization of novel densovirus infections among distinct invertebrate populations is of utmost importance to recognize outbreaks and accelerate responses. This is especially important in agricultural populations whose infections pose tremendous risk of interspecific spillover and economic devastation. Herein, we describe an outbreak of densovirus infection with high mortality in a commercial mealworm farm in 2020. This report focuses on the characterization of the molecular, bright-field, and electron microscopic (EM) features of this infection and its clinical significance.

Materials and Methods

Clinical History

Problems began when a large commercial insect breeder was unable to raise larvae of YMW beetles. Anecdotally, the disease was first observed in 5- to 6-week-old post-hatching larvae, 3 to 5 weeks before the average harvesting age. YMW larvae presented with lethargy, size variability, cessation of eating, and "spinning" prior to death. All YMW larvae were affected and died (100% mortality) before reaching the harvesting size. These YMW larvae were fed a proprietary diet on which the farm had previously yielded good success. The feed was tested for various organophosphorus insecticides, which were not detected. Due to the progression of the disease, which affected various instars and presumably multiple production cycles, the farmer halted YMW larvae production practices. After several months of farming interruption and total reconstruction of the facilities, the breeder eventually resumed normal production of YMWs.

Histological Examination

YMW larvae were submitted for diagnostic investigation at both early and late development instars. Specimens were fixed in 10% neutral-buffered formalin for a minimum of 24 hours. Sagittal and coronal sections were taken from 15 affected and 5 unaffected individuals at the levels of the head, thorax, and abdomen. These 3 to 4 mm sections were routinely processed, embedded in paraffin wax, and stained with hematoxylin and eosin.[16] Feulgen staining for "in-situ" demonstration of DNA was performed on selected sections.[6]

Electron Microscopy

For detection, identification, and quantification, viruses were extracted, cleaned, concentrated, and contrasted using a modified nebulization method originally described by Cruickshank et al.[9] Briefly, YMWs were frozen at –80°C. To extract the virus from the tissue/cellular compartments, YMWs were subjected to 2 freeze/thaw cycles before bead-mill homogenization in a Bead Ruptor 12 (Omni International) at 5 m/s velocity for 45 seconds. The homogenate was then suspended in 15 mL of double-distilled water. Removal of macrodebris from this suspension was achieved by decantation via low-speed centrifugation at 2000*g* for 10 minutes at 30°C. The supernatant was filtered with a series of 5.0, 1.2, and 0.8 μm syringe filters (Fisher Scientific) to remove prokaryotes and microdebris. The supernatant was then subjected to ultracentrifugation at 285,000*g* for 110 minutes at 5°C (Optima L-80XP Ultracentrifuge; Beckman Coulter). The resulting supernatant was discarded and the pellet containing concentrated virus was resuspended in 200 μL of boiled double-distilled water. Next, a 2:1:1 dilution of virus pellet-1% sodium phosphotungstate solution (pH 6.8)-bovine serum albumin contrast was established. For viral screening, 100 μL of this mixture was micro-aerosolized onto a 200-mesh formvar/carbon-coated electron microscope grid (Electron Microscopy Sciences) using a glass nebulizer. For viral quantification, 1 μL of the 2:1:1 mixture was applied as a drop to an Alcian blue–treated 200-mesh formvar/carbon-coated electron microscope grid (Electron Microscopy Sciences). The detected virus was identified by finding repetitive profiles with consistent dimensions, morphological features, and structural characteristics that match the dimensions and features accepted and published by the Report of the International Committee on Taxonomy of Viruses.[19]

To quantify the amount of viral particles per gram of tissue, the number of viruses in a known area was calculated.[17] Enumerations of viral particles in a total of 20 individual 0.35 μm^2 areas ("sections") were performed and averaged. This enabled an estimation of the total number of viral particles on a single 3-mm diameter grid, based on its calculated surface area of 7.1 mm^2 (Electron Microscopy Sciences). Even distribution of viruses on the grid was ensured by the presence of bovine serum albumin in the suspension-stain mixture. Because this grid was covered by a known volume of viral pellet suspension (0.5 µL), the concentration of viral particles in the entire suspension could be determined. From here, the number of viral particles present in the known weight of mealworm tissue processed was estimated and scaled to determine the approximate number of viral particles contained in 1 g of mealworm tissue. A formula is provided below:

$$\frac{No.\ of\ Viral\ Particles}{Section\ Area} \times \frac{Grid\ Area}{Suspension\ Drop\ Volume} \times \frac{Total\ Suspension\ Volume}{Tissue\ Weight}$$

To analyze the tissue ultrastructure, whole bodies of 3 diseased YMWs and 3 unaffected individuals were fixed in Karnovsky's fixative (3% glutaraldehyde and 2% formaldehyde in 0.1M phosphate buffer, pH 7.4). Coronal sections of the body tissue were taken in 2 to 3 mm segments at 4 levels: head (1 section), thorax (2 sections), abdomen (2 sections), and podal appendages. These sections were postfixed with 1% osmium tetroxide in 0.1 M sodium cacodylate buffer. Samples were processed as described elsewhere.[1] Briefly, samples were dehydrated in a 25% to 100% ethyl alcohol gradient series for 2 hours using an automated tissue processor (Leica Microsystems). The tissue was then infiltrated with 1:1 and subsequently 3:1 EMbed 812 resin:propylene oxide for 1 and 2 hours, respectively. The tissue was then infiltrated with 100% resin for 3 hours before embedding and incubation at 58°C for 24 hours to polymerize the resin (all reagents were from Electron Microscopy Sciences). Embedded samples were trimmed and sectioned on a Leica UC7 ultramicrotome (Leica Microsystems). One-micrometer thick sections were mounted on glass slides and stained with toluidine blue to select areas of interest. From the selected areas, thin sections (70–90 nm) were obtained and collected on a 100-mesh nickel grid (Electron Microscopy Sciences). Grids were contrasted with 5% uranyl acetate for 20 minutes and Satos' lead citrate for 6 minutes. All samples were visualized using a JEOL 1400Plus transmission electron microscope (JEOL LTD). Images were obtained and analyzed using a OneView Camera Model 1095 with the Gatan Microscope Suite 3.0 (Gatan Inc).

Virus Sequence

Total nucleic acid was extracted from 200 µL of the resuspended EM pellet using the MagMax Pathogen RNA/DNA kit (Fisher Scientific) following the recommendations of the manufacturer. The extracted DNA was purified using AMPure XP beads (Beckman Coulter) and used as input to a library generated with the Ligation Sequencing Kit SQK-LSK109 (Oxford Nanopore Technologies [ONT]). First, DNA was end-repaired using the NEBNext Ultra II DNA End Prep and Repair kit (New England Biolabs), purified using AMPure XP beads in a ratio of 1:1 volume of beads per sample, and eluted in 30 µL of nuclease-free water. Sequencing adapters (AMX; ONT) were ligated to the DNA using NEBNext Quick T4 DNA ligase (New England Biolabs) by incubation at room temperature for 10 minutes. The adapter-ligated DNA library was purified with AMPure XP beads in a ratio of 1:2.5 volume of beads per sample, followed by 2 washes with S Fragment buffer (ONT) and elution in 7 µL of elution buffer (ONT). The library was loaded onto an FLO-MIN106 9.4 Flowcell on a GridION sequencer (ONT). Prior to starting the run, the sequencing kit SQK-LSK109 with barcoding expansion pack EXP-NBD196 and the "super accuracy" basecaller were selected in the MinKNOW data analysis software. After sequencing for 24 hours, FASTQ files containing "pass" reads (Q-score ≥10) were loaded into Geneious Prime (version 2022.1.1) and mapped to a reference densovirus genome (GenBank accession MT138240) using the MiniMap2 plugin. Using the mealworm densovirus genome sequence, as well as all densovirus whole genomes available in GenBank, a multiple sequence alignment was produced using the MUSCLE algorithm in Geneious. Phylogenetic analysis using a maximum likelihood method was performed with the program MEGA (version 11.0.11). The Hasegawa-Kishino-Yano (HKY) model of nucleotide (nt) substitution with gamma distributed rates was used, and bootstrap values were calculated using 1000 pseudo-replicates.

Results

Gross and Histological Findings

Upon gross examination, YMW larvae infected with densovirus presented with variably underdevelopment curved bodies and multifocal-to-generalized, dark cuticular discoloration (Fig. 1a). Organs and body tissue were soft, discolored, and reduced in volume when compared with those unaffected. Histologically, the lesions in infected YMWs were characterized by cytoplasmic and nuclear enlargement (cytomegaly and karyomegaly) with InI bodies and death of epithelial cells of the cuticular epidermis, pharynx and esophagus (foregut), rectum (hindgut), and respiratory tubules—tracheae and tracheoles (Figs. 1–3). All affected larvae examined were pharate instars. While the old cuticle was unshed (Fig.1b, c), the new cuticle was thin and undulated (Fig. 1e, h). Segmentally, the infected epidermis was 2-to-5 times thicker than the unaffected epidermis. Infected epidermal cells had cytoplasmic elongation. Their nuclei were at different levels, giving the epidermis an appearance of a pseudostratification or hyperplasia (Fig. 1d–h). On hematoxylin and eosin–stained preparations, InIs varied from basophilic to eosinophilic (Fig. 1e–h). The cells' nuclei were severely enlarged, and the inclusions replaced or displaced the chromatin to the nuclear margin (Fig. 1f, g).

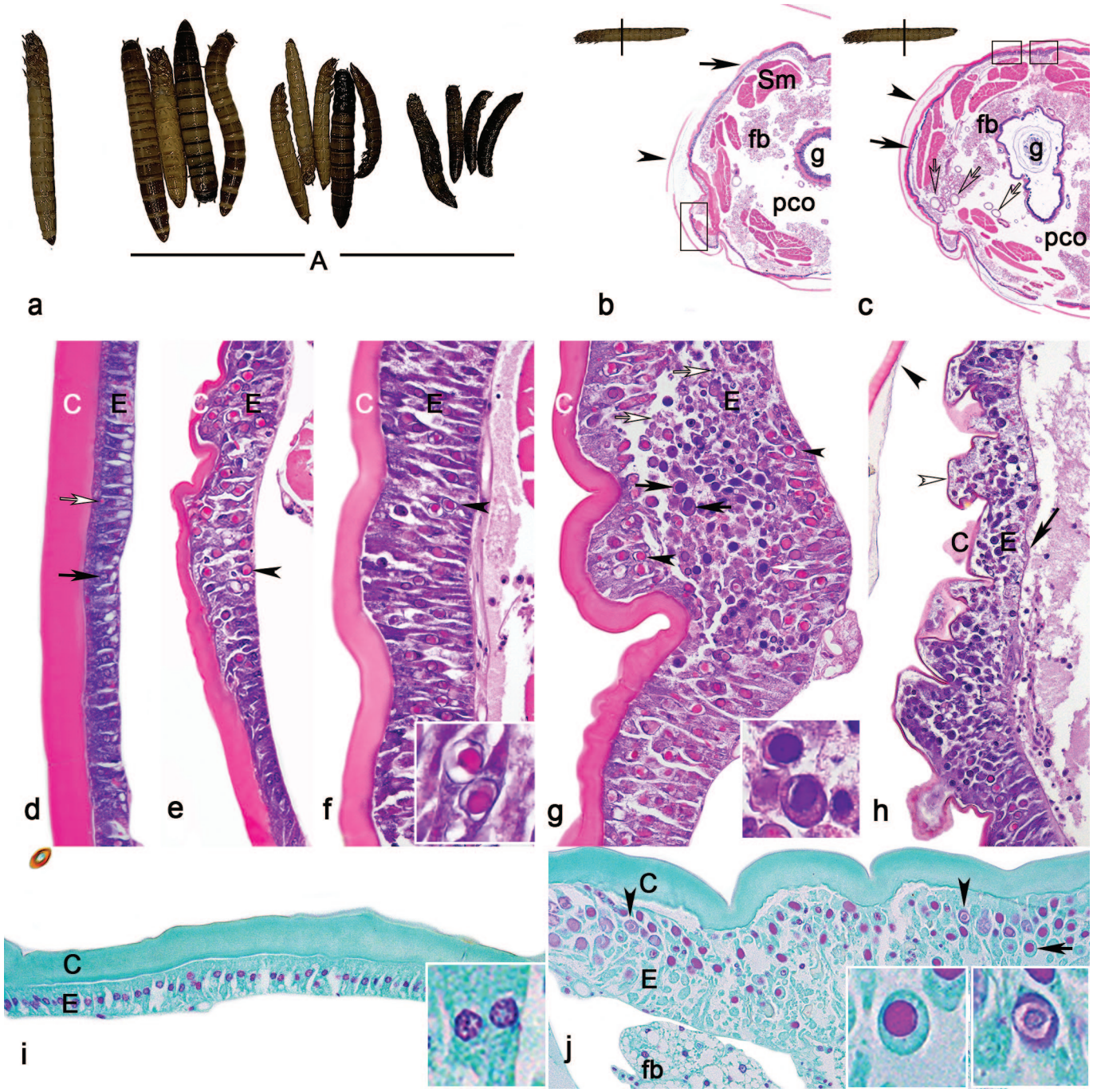

Figure 1. *Tenebrio molitor* larvae infected with densovirus. (a) On the right, infected larvae at different development instars (A) presenting variable degrees of dehydration and generalized dark discoloration compared with one unaffected individual on the left. (b, c) Cross sections of larvae infected with densovirus. Subgross images at the levels of the proximal (b) and distal (c) midgut depict the retention of an unshed cuticle (arrowhead), which is above a thin and undulate new cuticle. Open arrows indicate tracheal tubes; Sm, skeletal muscle; fb, fat body; pco, pseudocoelom; g, midgut. Boxes indicate areas highlighted in (e), (f), and (g). Hematoxylin and eosin (HE). (d) Unaffected integument with an eosinophilic cuticle (C) and columnar epidermal epithelium (E). These cells have a centrally located nucleus with coarse marginated chromatin (black arrow), eosinophilic secretory granules (white arrow), and basilar-located cytoplasmic vacuoles. HE. (e)–(h) Progression of epidermal cell lesions in larvae infected with densovirus; magnification of areas of the integument highlighted in (b) and (c). HE. A variably thin and undulate cuticle (C) is overlying infected epidermal cells (E). Infected epidermal cells are detached and enlarged, mildly in (e) to severely in (f) and (g). As is obvious in (h), individualized, infected cells between the cuticle (C) and basal lamina (black arrow) are suspended in proteinaceous fluid. Note the thick, unshed old cuticle (black arrowhead) compared with a thin, undulate new cuticle (open arrowhead). The nuclei of infected epidermal cells are enlarged due to eosinophilic and basophilic intranuclear inclusions. While eosinophilic inclusions (black arrowheads) predominate in (e) and (f), basophilic inclusions (black arrows) are present in (g) and (h). (e)–(g) Eosinophilic inclusions are rounded to polyhedrals surrounded by a clear hollow with chromatin displaced to the margin (arrowheads). (f) Inset: magnification

of eosinophilic inclusion. (g) Basophilic inclusions occupy the full area of the nucleus with indistinct margins of chromatin (black arrows). Inset: magnification of basophilic inclusion. (i) Unaffected integument, centrally located nuclei of epidermal cells display a bright pink reaction. Inset: magnification of 2 nuclei. Feulgen reaction correlates with a coarse distribution of the chromatin. Feulgen stain. (j) Infected integument, consecutive section of (g) stained with Feulgen. A significant number of inclusions have a homogeneous, positive bright pink reaction, which correlates with basophilic inclusions (black arrows in (g) and (j)). In contrast, a faint Feulgen reaction correlates with eosinophilic inclusions (black arrowheads in (f) and (j)). C, cuticule; fb, fat body lobe. Inset: magnification of a positive Feulgen reaction of a basophilic inclusion (right) in contrast to a faint reaction of an eosinophilic inclusion (left).

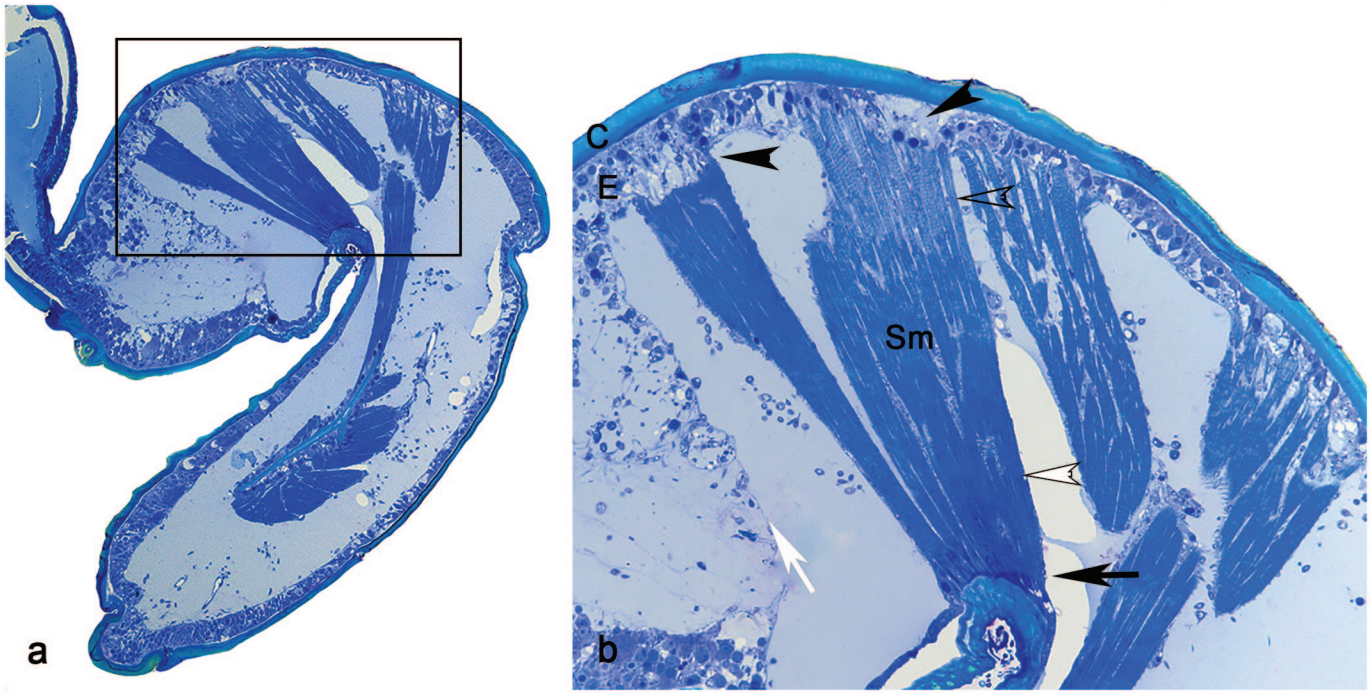

Figure 2. *Tenebrio molitor* larvae infected with densovirus. Leg preparations embedded in plastic and stained with toluidine blue. (a) Diffusely, epidermal cells are infected with densovirus. Note the interstitial space filled with proteinaceous exudate and hemocytes. (b) Magnification of the box in **(**a). The infected epidermal cells (E) are detached from the cuticle. A detachment of an intrinsic leg muscle due to death of epithelial cells is highlighted with black arrowheads. The black arrow shows inserted muscle at the button. Hypercontracted and hyperstretched muscle fiber segments are indicated by a white arrowhead and open arrowhead, respectively. The basement lamina is intact (white arrow).

There was individualization of epidermal cells and fragmentation of the nucleus and cytoplasm with formation of apoptotic bodies as later confirmed by transmission electron microscopy (TEM) (Fig. 1g, h). Eosinophilic inclusions had variable textures. While the homogeneous, basophilic inclusions correlated with strong, Feulgen-positive reactions, the eosinophilic inclusions presented faint Feulgen staining (Fig. 1j). Large numbers of basophilic intracytoplasmic granulations, interpreted as autophagy and heterophagy, were present in a significant number of epidermal cells, as later confirmed by TEM. Multifocal, epidermal cells of all segments of the body (head, thorax, and abdomen) were hypertrophied with InI and cell death. In advanced stages of infection, this lesion progressed to formation of vesicles between the endocuticle and basal lamina or subcuticular epidermal cell layer discontinuity (Fig. 1h). Vesicles contained individual epidermal cells, cellular and nuclear debris, and hemocytes floating in a proteinaceous fluid.

When epidermal cells that specialize in the skeletal muscle/cuticular attachment were infected and damaged by the virus, the skeletal muscle separated from its insertion with the cuticle—"muscle avulsion" (Fig. 2a, b). The detached skeletal muscle cell had variable degrees of degeneration with hyperstretching, hypercontraction, and necrosis and was observed in the muscle of the head, thorax, and legs, which included the craniomandibular muscle, dorsal and ventral longitudinal muscles, the dorso-ventral muscle, and muscles of the legs (Figs. 2a, b and 3b, c). Infected epithelial cells of the tracheae and tracheoles were hypertrophied (cuboidal transformation) and contained InIs, and some cells were undergoing cell death with fragmentation of the nucleus and cytoplasm (Fig. 3e, f). Similar to the cuticular epidermis, tracheal and tracheolar epithelial cells of all body segments and organs or systems, such as skeletal muscle and the nervous system, were affected (Fig. 3d–f). Other cells infected included pharyngeal, esophageal, and

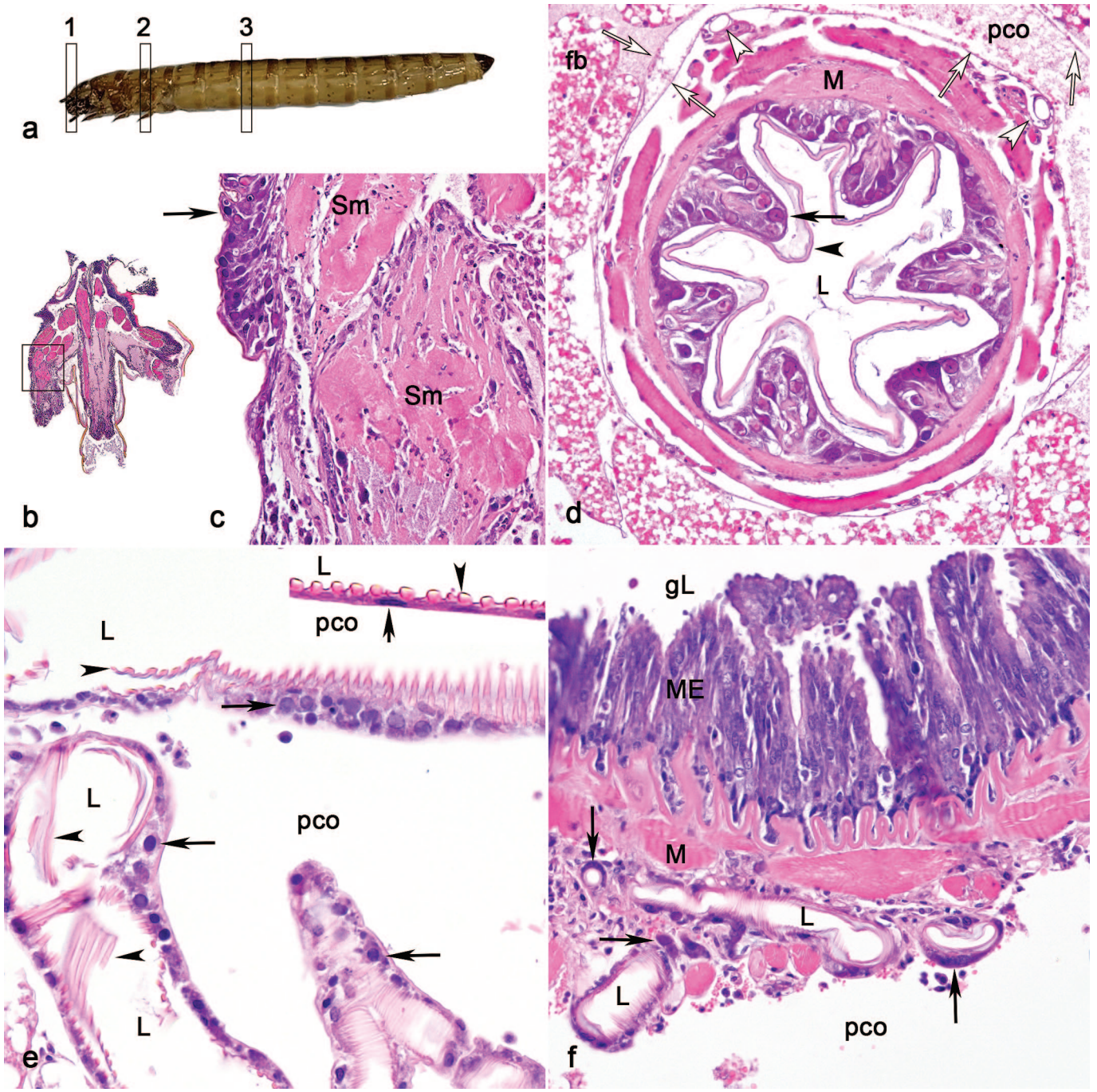

Figure 3. *Tenebrio molitor* larvae. (a) Unaffected larvae, sections included in the hematoxylin and eosin (HE) histological panel: 1, head; 2, thorax; 3, abdomen. (b) Infected larvae, section 1 in (a), subgross image of the head; the box indicates an area highlighted in (c). HE. (c) Diffusely, infected epidermal epithelial cells contain basophilic intranuclear inclusions (black arrow). The detached cuticle is not present. Skeletal muscles are segmentally necrotic (Sm). HE. (d) Section 2 in (a), esophagus, epithelial cells have eosinophilic intranuclear inclusions (black arrow). The cuticle is detached (black arrowhead). M, tunica muscularis; white arrowheads, tracheole; white arrows, basal lamina; pco, pseudocoelom; fb, fat body. HE. (e) Tracheal tubes, infected epithelial cells are cuboidal. Enlarged nuclei present basophilic inclusions (black arrows). The cuticle is detached (arrowheads). pco, pseudocoelom; L, tracheal tube lumen. Inset: Unaffected tracheal tube. Black arrow, epithelial cells; black arrowhead, cuticle; pco, pseudocoelom; L, tracheal tube lumen. HE. (f) Midgut, infected epithelial cells of tracheoles are hypertrophied, nuclei have basophilic inclusions (black arrows). L, tracheoles lumen; pco, pseudocoelom; M, tunica muscularis; ME, mucosal epithelium; gL, midgut lumen. HE.

rectal epithelial cells (Fig. 3d). There was a variable influx of hemocytes and proteinaceous fluid filling the pseudocoelom and legs (Fig. 2a, b). The viral infection was variable, but, in general, the head, thorax, and podal appendages were more severely affected. Other findings in infected YMW mealworm larvae not directly attributed to the viral infection were loss of

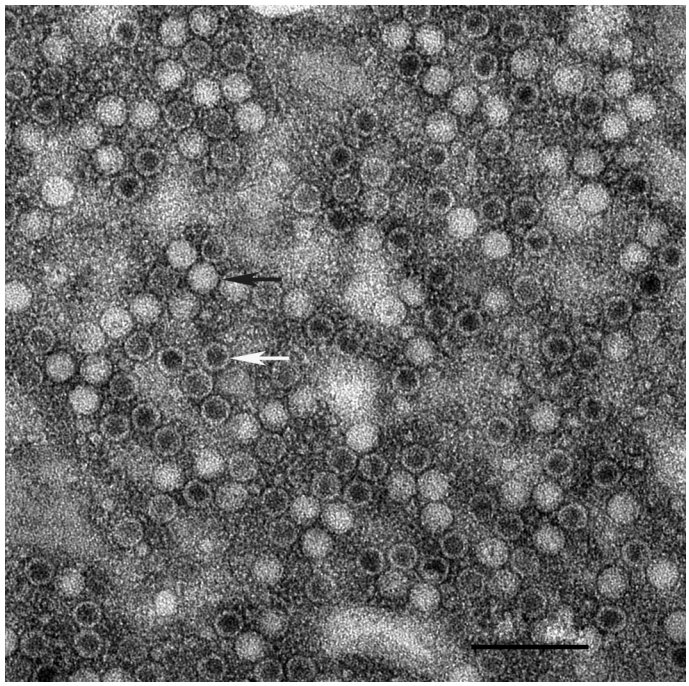

Figure 4. Densovirus virions recovered from *Tenebrio molitor* larvae. Transmission electron microscopy. Negative-contrasted, nonenveloped, round virus particles ranging from 23.79 to 26.99 nm in diameter. Comparable proportions of spheres (sealed, black arrow) and hollow (contrast-permeable, white arrow) virus particles are presented. Phosphotungstic acid. Bar = 100 nm.

mass and necrosis of fat body cells, and multiple hemocyte nodules.

Electron Microscopy Findings

Negative-contrasted virions were nonenveloped and icosahedral (Fig. 4). Densovirus virions varied in diameter from 23.79 to 26.99 nm, averaging 25.19 (SD = 0.94) nm. Frequently, hollow particles were observed (Fig. 4). Approximately 7×10^{12} densovirus virions per gram of tissue were recovered from *T. molitor* larvae. This estimation is based on an average of 361.5 viral particles enumerated per 0.35 μm^2 over a total of 20 individual 0.35 μm^2 areas and is provided under the assumption of even viral distribution on the grid and in the viral pellet suspension, as well as the assumption that the totality of viral particles was extracted from the sample tissue using the viral extraction methods employed.

Ultrastructurally, infected epidermal and epithelial cells of respiratory tubules presented with disintegration of the cuticular and intercellular anchoring junctions (Fig. 5a–d). Cells were rounded and displayed electron-dense mitochondria, laminar-to-circular ribosomal-lamellar complexes, and tubular-reticular complexes (Fig. 5a, b). Cells also had increased numbers of cytoplasmic vesicles. The nuclei were enlarged to double or triple the normal size, and the chromatin was replaced by a densovirus replication and assembly complex (DRAC). Infected epithelial cells at the "cuticle-epithelial cell-skeletal muscle attachment" detached from the endocuticle due to the disintegration of the muscle attachment fiber-hemidesmosome junction (Fig. 5c) and disintegration of the desmosome at the epithelial cell-skeletal muscle attachment. Degeneration of the tonofibrils was also present (microtubule; Fig. 5c). Respiratory epithelial cells presented similar ultrastructural changes to epidermal cells. However, DRAC in these cells was denoted by homogeneous accumulation of nucleocapsids compared with the DRAC of the cuticular epidermal cells (Fig. 5a, c, d). In epidermal cells, DRAC most commonly presented itself as a pleomorphic structure composed of a viral matrix that displaced and replaced the chromatin (Fig. 6). The virus matrices were fibrillar-granular with variable densities. The denser segment of the virus matrix, known as "virogenic stroma,"[13] was composed of short-to-long anastomosing streams, in which presumably maturing and mature virions were aggregating at the interface with the looser granular matrix spaces (Fig. 6a–c). DRACs evolved to form paracrystalline arrays (Fig. 6d–f), although these paracrystalline arrays were less common. In general, there was high variability of the DRAC morphology, which seemed dependent on both the stage of the cell infection and the proportion of dense and loose viral matrix. Figure 7 displays the most distinct features observed. Occasionally, nuclear fragments containing chromatin, virions, or paracrystalline arrays were found in the cytoplasm of infected and unaffected epithelial cells (Fig. 8a). Cell death was characterized by condensation of the cytoplasm and organelles, as well as nuclear envelope breakdown, blebbing, and fragmentation, which was interpreted as apoptosis (Fig. 8b–d). However, lysis of cytoplasm and nuclei was also observed (Fig. 8b). Nucleoli were displaced to the periphery and fibrillar and granular components were distinguishable (Figs. 7c, 8b). Free, small fragments of epidermal cell cytoplasm containing chromatin and/or viroplasm were interpreted as apoptotic bodies (Fig. 8b).

Virus Sequence

Whole-genome sequencing of the mealworm densovirus generated 296,000 reads, of which 71,338 reads mapped to a bird-associated densovirus reference strain (GenBank accession no. MT138240). The entire 5579 bp genome was detected at more than 10,000× depth of coverage. The consensus sequence was submitted to GenBank and given the accession number: MW628494. The genome contained 5 open reading frames (ORFs), 2 on one strand and 3 on the other (Fig. 9). ORF 1 (nt 2540–4321 complement strand) and ORF 2 (nt 4261–5172 complement strand) encode predicted structural proteins of 593 and 303 amino acids, respectively, while ORF 3 (nt 938–2539), ORF 4 (nt 945–1742), and ORF 5 (nt 392–904) encode predicted nonstructural proteins of 533, 265, and 170 amino acids, respectively. A phylogenetic analysis of the mealworm densovirus showed it to be closely related to several bird- and bat-associated densovirus, sharing 97% to 98% identity. Meanwhile, the nucleotide similarity to mosquito, cockroach, and cricket densoviruses was 55%, 52%, and 41%, respectively (Fig. 10).

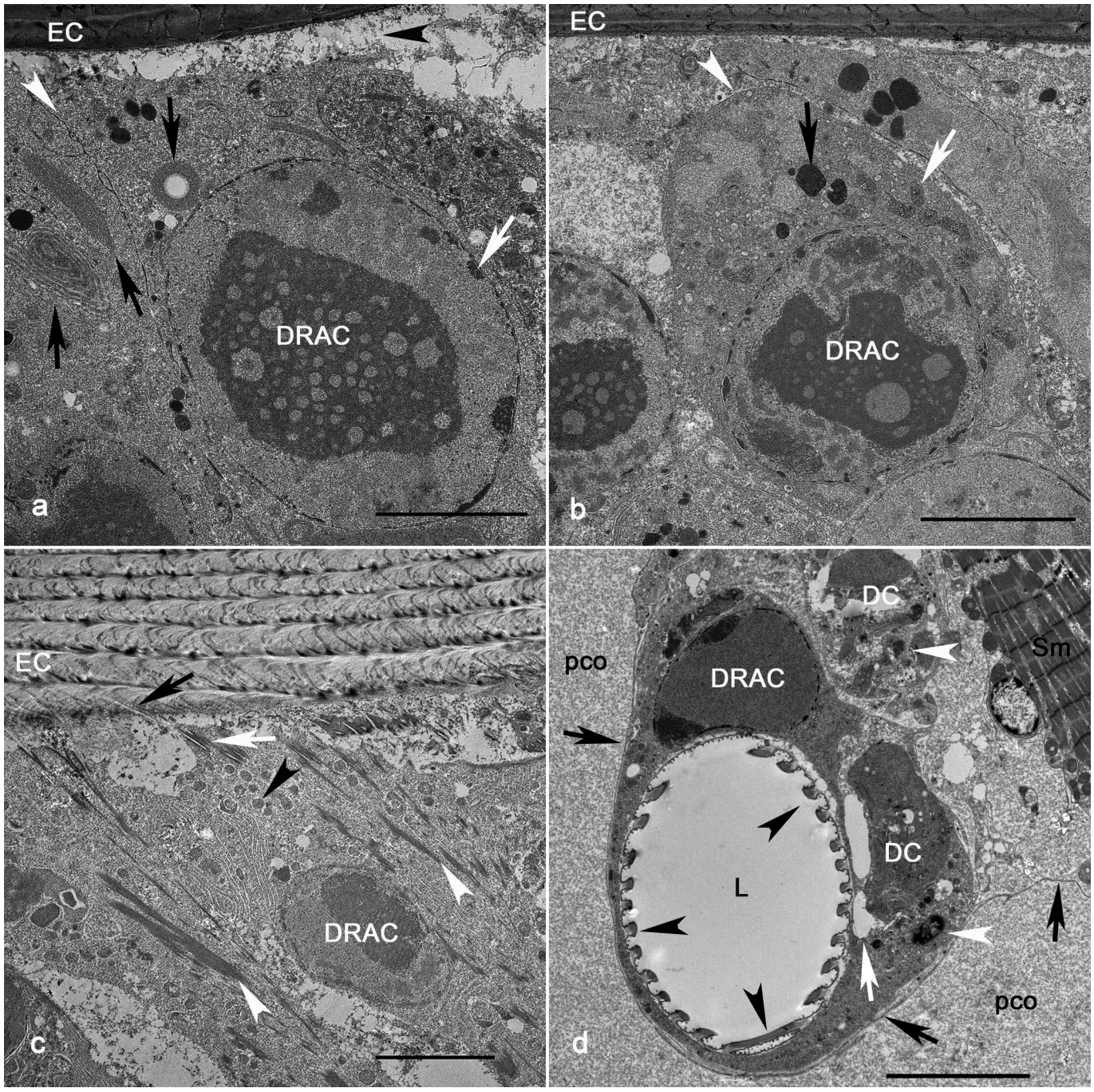

Figure 5. *Tenebrio molitor* larvae infected with densovirus. Transmission electron microscopy. (a) The epidermal epithelial cell contains a large nuclear densovirus replication and assembly complex (DRAC). Other cytopathic effects include endocuticular detachment due to the degradation of the anchoring junctions (black arrowhead) and cytoplasmic formation of circular and lamellar membranous bodies (black arrows). White arrowhead, plasma membrane; white arrow, nuclear membrane and chromatin; EC, endocuticle. Bar = 5 μm. (b) Epidermal epithelial cells are detached from the endocuticle and adjacent cells. The plasma membrane is indicated with a white arrowhead. Within its cytoplasm, there are electron-dense phagolysosomes (black arrow) and degenerated mitochondria (white arrow). Bar = 5 μm. (c) Infected epithelial cells at the "cuticle-epithelial cell-skeletal muscle insertion" are detached due to the disintegration of the muscle attachment fiber-hemidesmosome junction (black and white arrows, respectively). The nuclear chromatin is replaced by a DRAC. Degenerated tonofibrils and mitochondria are depicted with white and black arrowheads, respectively. Bar = 5 μm. (d) Tracheole, epithelial cells contain a nuclear DRAC that triplicates the size of a normal nucleus. Dead epithelial cells (DC) with nuclear fragments (arrowheads) are detaching from the cuticle (white arrow). L, lumen; black arrow, basement lamina; pco, pseudocoelom; Sm, skeletal muscle. Bar = 5 μm.

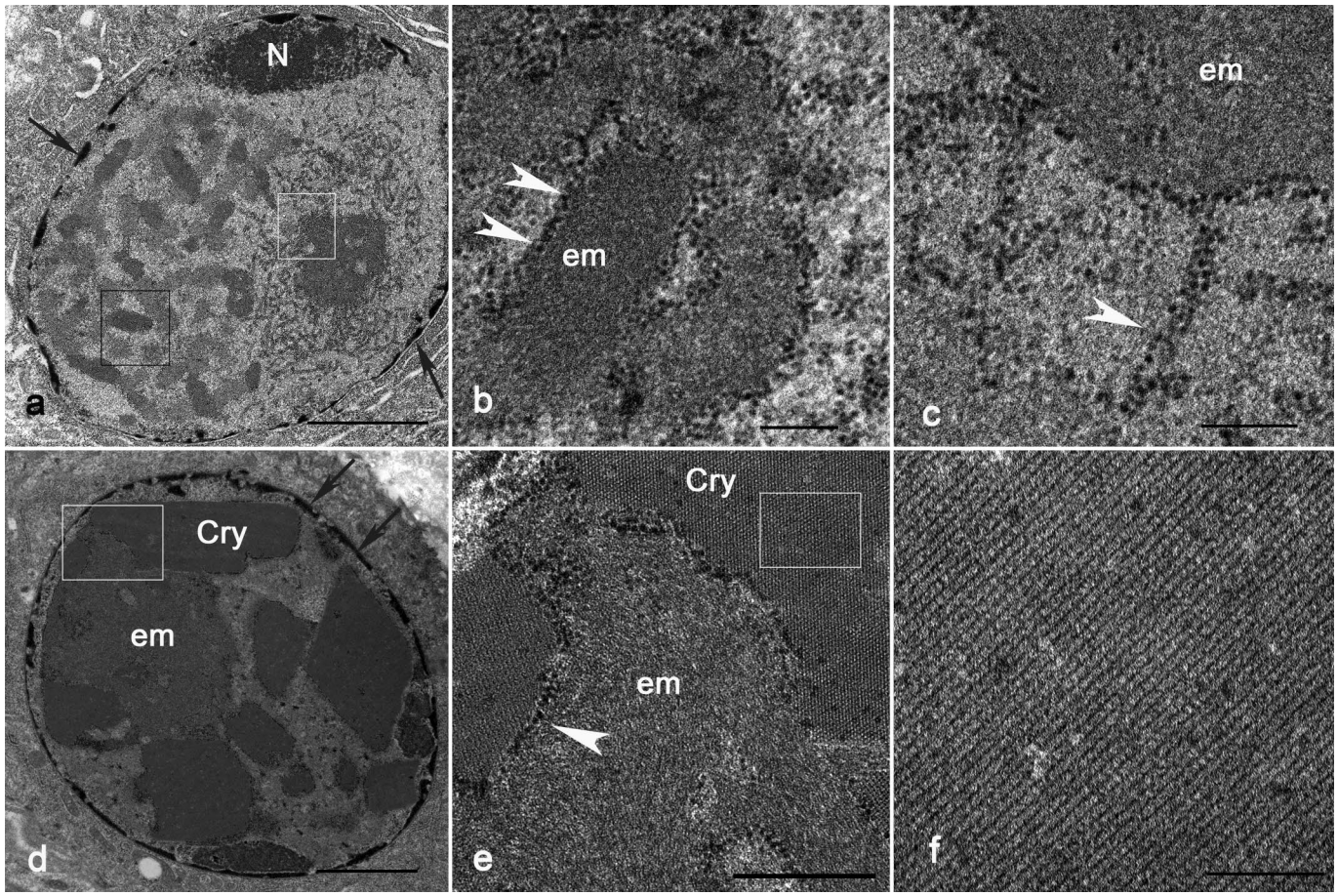

Figure 6. *Tenebrio molitor* larvae infected with densovirus. Transmission electron microscopy. (a) Nucleus of an epidermal epithelial cell contains a densovirus replication and assembly complex (DRAC), which has displaced the chromatin to the margin (black arrows). These DRACs are composed of anastomosing streams of viral matrices of variable electron densities. On the left is a compacted virus matrix radiating cordons of assembled densovirus particles. N, nucleolus. Bar = 2 μm. (b) Magnification of black box in (a). Densovirus particles (white arrowheads) are assembled at the margin of electron-dense fibrillar matrix (em) streams. Bar = 200 nm. (c) Magnification of white box in (a). Densovirus particles (white arrowhead) forming long cords are assembled at the margin of the nucleolus-like compacted aggregate of electron-dense fibrillar matrix (em). Bar = 200 nm. (d) Nucleus of an epidermal epithelial cell displaying DRAC with paracrystal formation (Cry) that comprises approximately 40% of the nuclear volume. em, electron-dense matrix. Bar = 200 nm. (e) Magnification of the box in (d). Densovirus particles (white arrowhead) are assembled at the margin of an electron-dense fibrillar matrix (em) stream. Cry, paracrystal formation. Bar = 500 nm. (f) Magnification of the box in (e). Paracrystalline formation. Bar = 200 nm.

Discussion

An outbreak of densovirus infection with high mortality in a mealworm farm is described. The initial diagnosis was based on cellular hypertrophy (cytomegaly and karyomegaly) with InI bodies and death of epithelial cells of the epidermis, pharynx, esophagus, rectum, and tracheal system on histological examination, as well as the detection of virions consistent with viruses of the family *Parvoviridae* by direct TEM. Further genomic characterization shows that the detected YMW virus belonged to the genus *Ambidensovirus* of the subfamily *Densovirinae*, a group characterized by its unique bidirectional ("ambisense") transcription.[8]

A phylogenetic comparison of the whole genome placed this virus among several closely related densoviruses detected in the feces of various birds and bats. Unfortunately, given the broad diets of these insectivorous hosts, it is impossible to ascertain whether mealworms or other unrelated insect species may have been the sources of the described densovirus. However, a densovirus recently identified as the causative agent of a superworm (*Zophobos morio*) mortality event at a Moscow zoo[39] showed 97% nucleotide identity across 774 bp of the ORF 3 region to the mealworm densovirus in this study. The next most closely related densovirus of insect origin is a mosquito densovirus (MH188043), which only shares 55% nucleotide identity with the mealworm densovirus. In comparison, the mosquito densovirus genome is significantly smaller (by over 2000 bp), and its organization is vastly different, containing a truncated structural protein gene (ORF1) and completely lacking a nonstructural protein (ORF5). There are currently relatively few complete insect densovirus genomes available in Genbank. This makes it difficult to draw firm

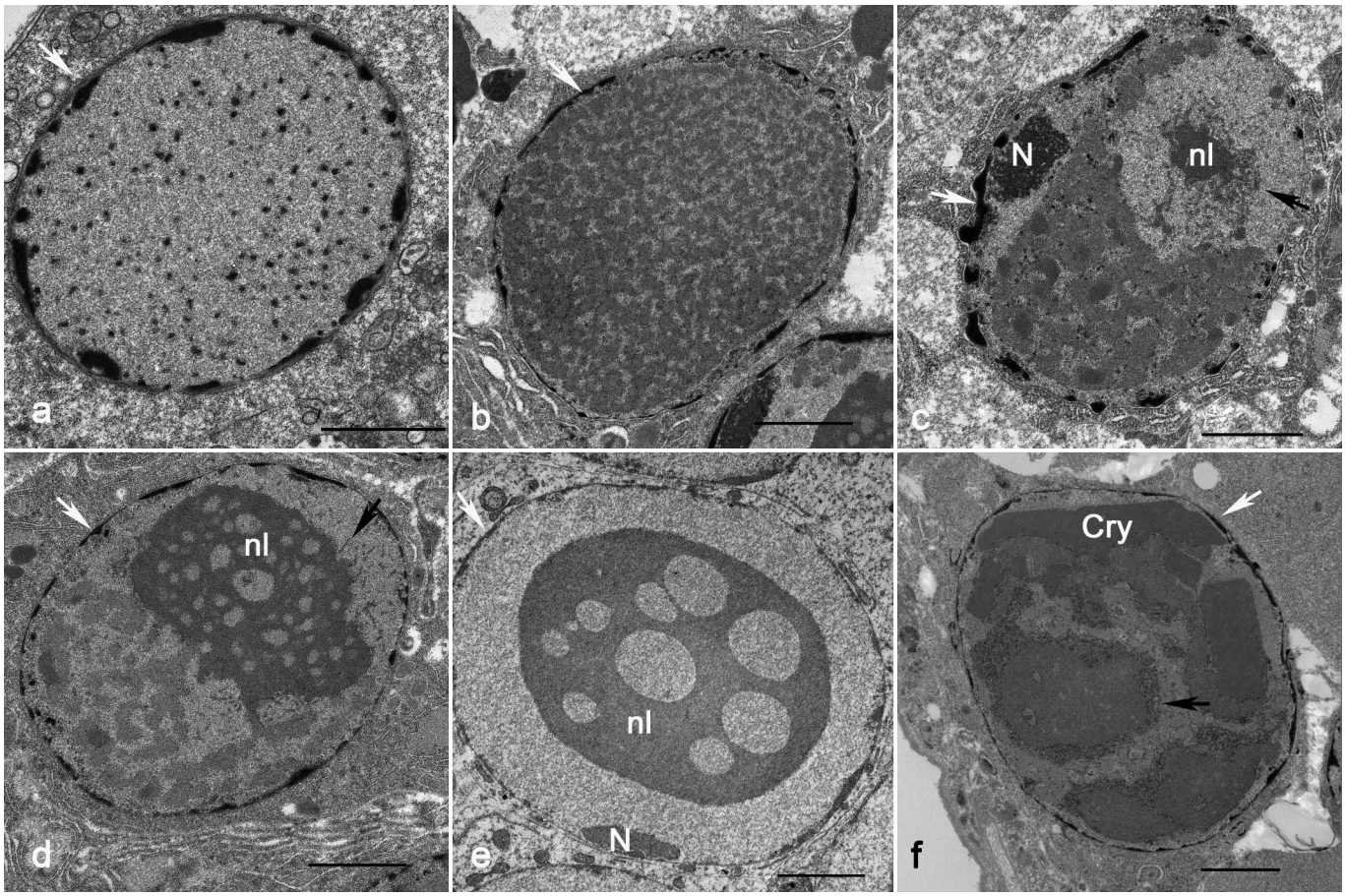

Figure 7. *Tenebrio molitor* larvae infected with densovirus. Transmission electron microscopy. (a–f) Different conformations of the densovirus replication and assembly complex (DRAC). Note the variation of electron density, texture of the virus matrix, and chromatin at the periphery (white arrow). A nucleolus (N) is present only in (c) and (e). A nucleolus-like aggregation of dense matrix (nl) is present in (c)–(e). Densovirus virions are marked with black arrows in (c), (d), and (f). Paracrystal (Cry) formation is obvious in (f). Bars = 2 μm.

conclusions about their relationships, and it is likely that the taxonomic groupings within the subfamily will be further refined as more genomes are described. As this is the first whole-genome characterization of a YMW densovirus, we propose the name *Tm*DNV.

The current outbreak of densovirus in *T. molitor* larvae achieved 100% mortality. This is consistent with 90% to 100% mortality reported in densovirus outbreaks affecting *Z. morio*[39] and house crickets (*Acheta domesticus*) in Europe and in the United States.[36]

Introduction of diseased insects or persistently infected individuals is the most probable origin of the current outbreak,[39] although the exact mechanism of the virus' introduction to the mealworm rearing facility and disease predisposing factors are impossible to determine as epidemiological information remains largely anecdotal. Experimentally, it has been demonstrated that a colony of mid-age-to-young *Z. morio* larvae can collapse within 1 to 2 months after the initial infection. Larvae usually die within a few days of infection; however, surviving larvae can evolve to the pupal and adult stages of their life cycle. Densoviruses are actively infectious for more than 18 months after the death of their host insect.[39] We estimated by TEM that perished larvae of *T. molitor* contain 7×10^{12} particles per gram of larvae tissue (equivalent to 5 dark, dry larvae). This is an extraordinary number of virus particles per larval carcass that, if aerosolized, could contaminate the surrounding environment and fomites, leading to effective dissemination in and across rearing facilities for extended periods of time.[35] The large quantity of viral particles generated in dead larvae permits the use of direct TEM as a rapid diagnostic screening method, preceding molecular tests or due to their unavailability. One inconsistency, which may limit the diagnosis of the virus on phosphotungstic acid–contrasted direct TEM preparation, is the large dimensional range reported for *Densovirinae* at 17 to 27 nm in diameter.[38] These dimensions overlap in the higher range with viruses of the order Picornaviruses and in the lower range with viruses of the family *Circoviridae*.[19] Densovirus particles in the current outbreak in *T. molitor* averaged 25.19 nm in diameter, ranging from 23.79 to 26.99 nm.

A significant contribution of our report is the detailed histological and ultrastructural characterization, which confirms densovirus as the cause of high mortality in *T. molitor*. The *Tm*DNV primarily affects epithelial cells of the cuticular

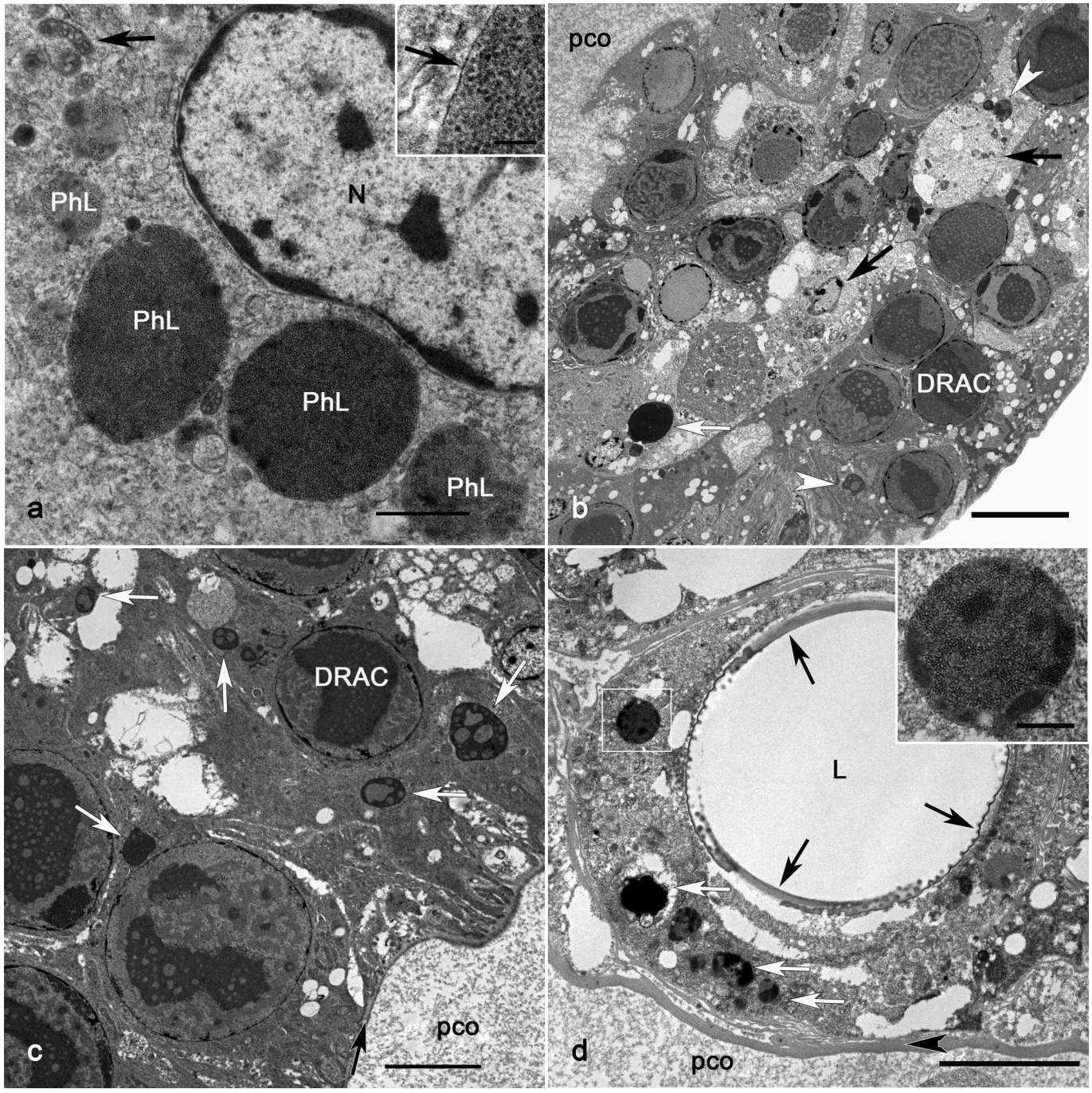

Figure 8. *Tenebrio molitor* larvae infected with densovirus. Transmission electron microscopy. (a) In the cytoplasm of an apparently uninfected epidermal cell are small and large phagolysosome (PhL)-containing densovirus particles. Its oval nucleus has clumped and marginated heterochromatin. Black arrow, mitochondrion. Bar = 1 µm. Inset: Magnification of a phagolysosome containing densovirus particles lined by membrane (black arrow). Bar = 125 nm. (b) The epidermis is expanded by up to 5 layers of nuclei, which contain intranuclear, heterogeneous densovirus replication and assembly complexes (DRACs). While numerous cells have small nuclear/DRAC fragments (white arrowheads) within their cytoplasm, larger fragments of nuclei/DRAC with vestigial amounts of cytoplasm are free (white arrow). Some cells have swollen cytoplasm and nuclear lysis (black arrows). Bar = 10 µm. (c) Nuclear/DRAC fragments of various sizes are present within the cell cytoplasm (white arrows). Black arrow, basal lamina; pco, pseudocoelom. Bar = 5 µm. (d) Tracheolar epithelial cells undergoing death are detaching from the cuticle (black arrows). The cytoplasm contains nuclear fragments in which the chromatin was replaced by virus particles (white arrows). L, lumen; pco, coelom; black arrowhead, basement lamina. Inset: Magnification of the white box in (d), nuclear fragment containing myriad virus particles. Bar = 500 nm.

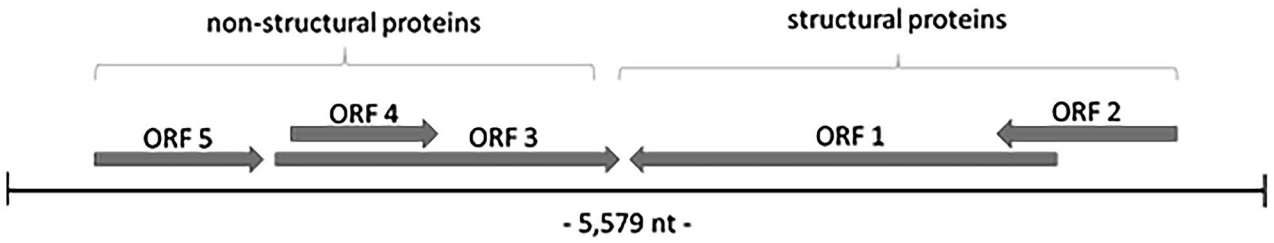

Figure 9. Genomic organization of *Tenebrio molitor* densovirus (*Tm*DNV) indicating the location and direction of transcription for each of the 5 open reading frames (ORFs).

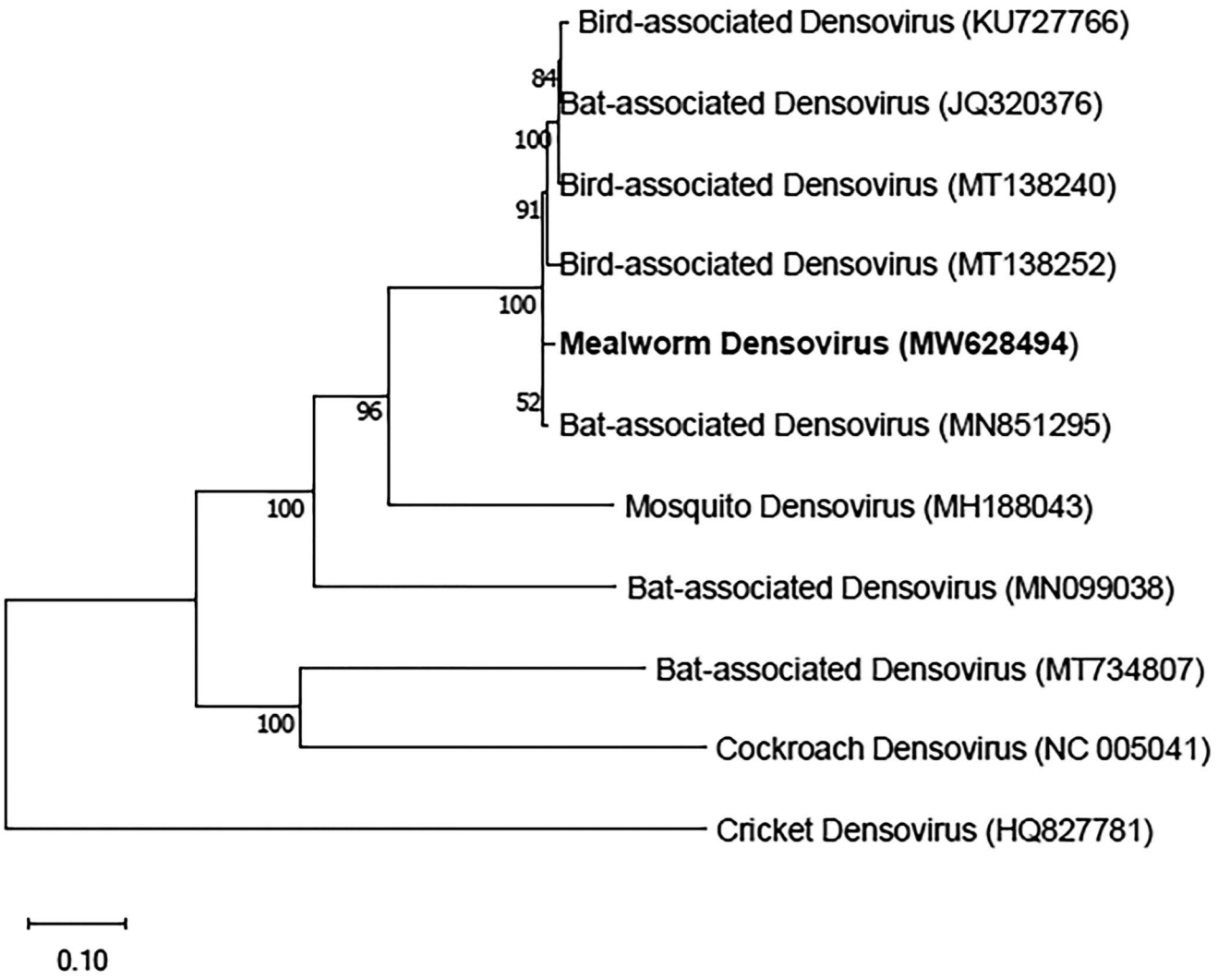

Figure 10. Phylogenetic analysis of the mealworm densovirus (*TmDNV*) whole-genome sequence in relation to other insect densoviruses. The numbers at the nodes represent bootstrap confidence values for 1000 replicates based on maximum likelihood analysis.

epidermis, tracheae, and tracheoles, in addition to the pharynx, esophagus, and rectum. These are all cuticular-secreting epithelial cells, which suggests that this *Tm*DNV is primarily epitheliotropic. On hematoxylin and eosin preparations, cytomegaly and karyomegaly with basophilic and eosinophilic inclusions of these cells are widely found in the head, thorax, and abdomen of early and late larval instars. Because tracheoles are distributed throughout the body of the larva,[30] densovirus inclusions can be

observed in the skeletal muscles, nervous systems, fat bodies, Malpighian tubules, gastrointestinal tracts, dorsal vessels (heart), and silk glands of severely infected individuals. These findings diverge with polytrophic members of the genus *Ambidensovirus*, which can efficiently replicate in most larval, nymphal, and adult tissues. Nevertheless, similar to polytrophic *Ambidensovirus, Tm*DNV does not affect the midgut glandular epithelium of its host.[8,20,22,25,28,36]

Generally, clinical signs reported in lethally infected natural hosts are anorexia and lethargy followed by flaccidity, which progresses to paralysis, slow "melanization," and death.[38] These clinical signs are consistent with those reported in the current densovirus outbreak in *T. molitor*; however, the terminology used should be revised to avoid imprecisions. Thus, based on the nature and extension of the lesions in densovirus-infected *T. molitor*, it can be suggested that clinical signs should primarily reflect an impairment of the locomotion, food ingestion, respiration, and body water balance as a consequence of the infection of epithelial cells of the epidermis, foregut and hindgut, and tracheal system. Locomotion impairment due to significant lesion was the result of the death of epidermal cells at the skeletal muscle-cuticular attachment, causing intrasegmental and intersegmental muscle detachment. Detached muscle fibers ("muscle avulsion") presented hyperstretching and hypercontraction followed by degeneration and necrosis. Skeletal muscle detachment affecting craniomandibular muscles results in an inability to prehend food rather than "anorexia," which would imply a lack of appetite.[44] Furthermore, multifocal infection of dorso-ventral muscles, dorsal and ventral longitudinal muscles, and intrinsic and extrinsic leg muscles will cause asymmetrical and asynchronous locomotion that generates swirling, rolling, and nonambulatory larva rather than paralysis and/or ataxia, which are terms usually associated with neurological impairment.[5,42] Respiration impairment is due to skeletal muscle lesions that interfere with larval breathing by affecting convective gas transport, which variably depends on muscle contractions.[3,29,30] In addition, the death of tracheolar epithelial cells may further impair larval respiration by interfering with O_2/CO_2 transport and exchange.[7] In terrestrial insects, transpirational water loss through the integumentary and respiratory systems accounts for more than 60% of the body's water loss.[3] Loss of integrity of the cuticle and epithelial cells of the integumentary and tracheal systems in *T. molitor* larvae due to densovirus infection may not only cause dehydration via excessive water loss, but also secondary infection by bacteria and fungi as a result of the loss of their primary defense barrier against infection. One limitation encountered in this study was the interpretation of a dark discoloration presented by densovirus-infected *T. molitor* larvae. Further investigation into the mechanism of this change is suggested as there remains uncertainty to whether this is in fact hemocyte granule prophenoloxidase-mediated melanization or some other possible explanation, such as the collection of debris over an unshed and desiccated cuticle.

InI is the most important microscopical feature of the densovirus infection in *T. molitor*. InI observed on bright-field microscopy represents the DRAC observed on electron microscopy. The infection with *Tm*DNV induces homogeneous basophilic- and eosinophilic-texturized InIs. Feulgen staining confirmed the DNA-dominant nature of the basophilic InIs, which correlates with DRACs accumulating maturing and mature virions on TEM as is shown in Figs. 6d and 7a. On the other hand, a great number of eosinophilic-texturized InIs presented with a fainter staining after the Feulgen reaction, which correlates with DRACs shown in TEM photomicrographs in Fig. 7c–f. Eosinophilic-texturized inclusions represented DRACs that ultrastructurally displayed an evolving mixture of heterogeneous viral matrix, maturing and mature virions, and ribosomes. Viral matrix observed in DARC was composed of electron-dense fibrillar small-aggregating-to-long-anastomosing streams, which evolved into a large compact mass that resembles the shape of a "rotary dial" (Fig. 7e). Similar structures were described in early studies of *G. mellonella* infected with densovirus.[13] Later, H-1 parvovirus studies indicated that H-1 parvovirus–associated replication bodies, which are not uncommonly observed in DRAC in *T. molitor* (Fig. 7a), are composed of nucleolar fibrils and serve as the location of viral DNA replication.[10,32] Differentiating maturing and mature virions from ribosomes in the infected nucleus on conventional plastic-embedded preparations posed a challenge. However, the large number of virus particles recovered on direct TEM supports the observation that large quantities of round vesicles/particles of about 18 to 24 nm in diameter found within the DRAC were in fact maturing and mature densovirus virions rather than ribosomes.

The DRAC displayed a very pleomorphic morphology, which varied from accumulation of maturing and mature virions to dense virus matrix that mimicked nucleolar structures and paracrystalline arrays. This heterogeneous ("nucleolus-like") appearance of the DRAC is an important feature that characterizes and facilitates *Tm*DNV diagnosis at the ultrastructural level. Initial TEM studies on the *G. mellonella* densovirus demonstrated that the nucleoplasm is completely replaced by virions during the first 20 hours of infection.[13] As in other autonomous parvoviruses that depend on the S phase of the infected cells, *Tm*DNV replication and assembly is a unique and dynamic process that demands a deeper understanding.[14,31] Nonetheless, crystallization of the DRAC forming "paracrystalline arrays" was interpreted as the final stage of nuclear infection with densovirus in *T. molitor*. Numerous infected cells presented cytoplasmic membrane–bound vesicles containing virus particles or paracrystalline arrays. Intracytoplasmic paracrystalline arrays have been considered a distinct feature of *Densovirinae* infections.[8] The origin of the structures is not well understood, but it should be considered as a process of infected nuclear breakdown, heterophagia, or autophagia. Ultrastructural changes of the nuclei and cytoplasm in *Tm*DNV-infected epithelial cells suggest apoptosis as the mechanism of cell death, although studies on viruses of the *Parvoviridae* family suggest that the mechanisms of *Parvoviridae*-induced cell death are unique and complex, warranting further investigation.[4]

In conclusion, we describe an outbreak of densovirus infection in YMWs with high mortality. Sequence analysis identified a novel densovirus, which we named *Tenebrio molitor* densovirus. This virus is epitheliotropic, affecting cuticular epidermal, foregut and hindgut, and tracheal epithelial cells, which will directly or indirectly lead to body water loss and exoskeletal-muscular detachment. Clinical signs are presented as an inability to prehend food, abnormal and asymmetric locomotion evolving to nonambulation, dehydration, and death. The diagnosis can be made histologically through the identification of massive epidermal cell death, cytomegaly, and karyomegaly with InI bodies. Detection of small round viral particles by direct transmission electron microscopy and/or molecular fingerprints of the virus in larvae tissue will confirm the disease.

Acknowledgements

We thank Mrs Karen Sverlow for the excellent histological and histochemical preparations, as well as Mrs Christina Heard and Mrs Rosa Mañalac for the outstanding transmission electron microscopy preparations necessary to complete this work.

Declaration of Conflicting Interests

The author(s) declared no potential conflicts of interest with respect to the research, authorship, and/or publication of this article.

Funding

The author(s) received no financial support for the research, authorship, and/or publication of this article.

ORCID iD

Aníbal G. Armién https://orcid.org/0000-0002-1870-9945

References

1. Armién AG, Wolf TM, Mor SK, et al. Molecular and biological characterization of a cervidpoxvirus isolated from moose with necrotizing dermatitis. *Vet Pathol*. 2020;**57**(2):296–310. doi:10.1177/0300985819891240
2. Bertola M, Mutinelli F. A systematic review on viruses in mass-reared edible insect species. *Viruses*. 2021;**13**(11):2280. doi:10.3390/v13112280
3. Beyenbach K, Piermarini P. Osmotic and ionic regulation in insects. In: Evans DH, ed. *Osmotic and Ionic Regulation: Cells and Animals*. Boca Raton, FL: CRC Press; 2009:231–293.
4. Caillet-Fauquet P, Perros M, Brandenburger A, et al. Programmed killing of human cells by means of an inducible clone of parvoviral genes encoding non-structural proteins. *EMBO J*. 1990;**9**(9):2989–2995. doi:10.1002/j.1460-2075.1990.tb07491.x
5. Caveney S. Muscle attachment related to cuticle architecture in Apterygota. *J Cell Sci*. 1969;**4**(2):541–559. doi:10.1242/jcs.4.2.541
6. Chieco P, Derenzini M. The Feulgen reaction 75 years on. *Histochem Cell Biol*. 1999;**111**(5):345–358. doi:10.1007/s004180050367
7. Chown SL, Nicolson SW. Metabolism and gas exchange. In: Insect Physiological Ecology: Mechanisms and Patterns. Oxford, England: Oxford University Press; 2004. doi:10.1093/acprof:oso/9780198515494.003.0003
8. Cotmore SF, Agbandje-McKenna M, Canuti M, et al; ICTV Report Consortium. ICTV virus taxonomy profile: parvoviridae. *J Gen Virol*. 2019;**100**(3):367–368.
9. Cruickshank JG, Berry DM, Hay B. The fine structure of infectious laryngotracheitis virus. *Virology*. 1963;**20**:376–378. doi:10.1016/0042-6822(63)90129-6
10. Cziepluch C, Lampel S, Grewenig A, et al. H-1 parvovirus-associated replication bodies: a distinct virus-induced nuclear structure. *J Virol*. 2000;**74**(10):4807–4815. doi:10.1128/jvi.74.10.4807-4815.2000
11. Dhar AK, Cruz-Flores R, Caro LFA, et al. Diversity of single-stranded DNA containing viruses in shrimp. *Virusdisease*. 2019;**30**(1):43–57. doi:10.1007/s13337-019-00528-3
12. Eilenberg J, Vlak JM, Nielsen-LeRoux C, et al. Diseases in insects produced for food and feed. *J Insects Food Feed*. 2015;**1**(2):87–102.
13. Garzon S, Kurstak E. Ultrastructural studies on the morphogenesis of the densonucleosis virus parvovirus. *Virology*. 1976;**70**(2):517–531. doi:10.1016/0042-6822(76)90293-2
14. Gil-Ranedo J, Hernando E, Riolobos L, et al. The mammalian cell cycle regulates parvovirus nuclear capsid assembly. *PLoS Pathog*. 2015;**11**(6):e1004920. doi:10.1371/journal.ppat.1004920
15. Grau T, Vilcinskas A, Joop G. Sustainable farming of the mealworm Tenebrio molitor for the production of food and feed. *Z Naturforsch C J Biosci*. 2017;**72**(9–10):337–349. doi:10.1515/znc-2017-0033
16. Gregor KM, Becker SC, Hellhammer F, et al. Histochemical staining techniques in Culex pipiens and Drosophila melanogaster (Diptera) with a comparison to mammals. *Vet Pathol*. 2022;**59**(5):836–849. doi:10.1177/03009858221088786
17. Hayat MA, Miller SE. *Negative Staining*. New York, NY: McGraw-Hill; 1990.
18. Jongema Y. List of edible insect species of the world. Laboratory of Entomology, Wageningen University. April 1, 2017. Accessed August 26, 2022. https://www.wur.nl/en/Research-Results/Chair-groups/Plant-Sciences/Laboratory-of-Entomology/Edible-insects/Worldwide-species-list.htm.
19. King AMQ, International Committee on Taxonomy of Viruses, International Union of Microbiological Societies. *Virus Taxonomy: Ninth Report of the International Committee on Taxonomy of Viruses*. New York, NY: Academic Press; 2012.
20. Kurstak E. Small DNA densonucleosis virus (DNV). *Adv Virus Res*. 1972;**17**:207–241. doi:10.1016/s0065-3527(08)60751-4
21. Lawal K, Kavle RR, Akanbi T, et al. Enrichment in specific fatty acids profile of Tenebrio molitor and Hermetia illucens larvae through feeding. *Future Foods*. 2021;**3**:100016. doi:10.1016/j.fufo.2021.100016
22. Li J, Dong Y, Sun Y, et al. A novel densovirus isolated from the Asian tiger mosquito displays varied pathogenicity depending on its host species. *Front Microbiol*. 2019;**10**:1549. doi:10.3389/fmicb.2019.01549
23. Li Y, Zádori Z, Bando H, et al. Genome organization of the densovirus from Bombyx mori (BmDNV-1) and enzyme activity of its capsid. *J Gen Virol*. 2001;**82**(Pt 11):2821–2825. doi:10.1099/0022-1317-82-11-2821
24. Liu K, Li Y, Jousset FX, et al. The Acheta domesticus densovirus, isolated from the European house cricket, has evolved an expression strategy unique among parvoviruses. *J Virol*. 2011;**85**(19):10069–10078. doi:10.1128/JVI.00625-11
25. Mukha DV, Chumachenko AG, Dykstra MJ, et al. Characterization of a new densovirus infecting the German cockroach, Blattella germanica. *J Gen Virol*. 2006;**87**(Pt 6):1567–1575. doi:10.1099/vir.0.81638-0
26. Myers JH, Cory JS. Biological control agents: invasive species or valuable solutions? In: Vilà M, Hulme P, eds. *Impact of Biological Invasions on Ecosystem Services. Invading Nature* (Springer series in invasion ecology). Cham, Switzerland: Springer; 2017:191–202. doi:10.1007/978-3-319-45121-3_12
27. Nakagaki BJ, Defoliart G. Comparison of diets for mass-rearing Acheta domesticus (Orthoptera: Gryllidae) as a novelty food, and comparison of food conversion efficiency with values reported for livestock. *J Econ Entomol*. 1991;**84**:891–896.
28. O'Neill SL, Kittayapong P, Braig HR, et al. Insect densoviruses may be widespread in mosquito cell lines. *J Gen Virol*. 1995;**76**(Pt 8):2067–2074. doi:10.1099/0022-1317-76-8-2067
29. Pendar H, Kenny MC, Socha JJ. Tracheal compression in pupae of the beetle Zophobas morio. *Biol Lett*. 2015;**11**(6):20150259. doi:10.1098/rsbl.2015.0259
30. Raś M, Iwan D, Kamiński MJ. The tracheal system in post-embryonic development of holometabolous insects: a case study using the mealworm beetle. *J Anat*. 2018;**232**(6):997–1015. doi:10.1111/joa.12808

31. Salvetti A, Greco A. Viruses and the nucleolus: the fatal attraction. *Biochim Biophys Acta*. 2014;**1842**(6):840–847. doi:10.1016/j.bbadis.2013.12.010
32. Singer II, Rhode SL III. Ultrastructural studies of H-1 parvovirus replication. VI. simultaneous autoradiographic and immunochemical intranuclear localization of viral DNA synthesis and protein accumulation. *J Virol*. 1978;**25**(1):349–360. doi:10.1128/JVI.25.1.349-360.1978
33. Sinnuengnong R, Attasart P, Smith DR, et al. In vitro assembly of Penaeus monodon densovirus (PmDNV)-like particles produced in a prokaryote expression system. *Aquac Res*. 2017;**48**:4975–4981.
34. Steinfeld H. The livestock revolution—a global veterinary mission. *Vet Parasitol*. 2004;**125**(1–2):19–41. doi:10.1016/j.vetpar.2004.05.003
35. Sykes JE. *Canine and Feline Infectious Diseases*. St. Louis, MO: Elsevier/Saunders; 2014.
36. Szelei J, Woodring J, Goettel MS, et al. Susceptibility of North-American and European crickets to Acheta domesticus densovirus (AdDNV) and associated epizootics. *J Invertebr Pathol*. 2011;**106**(3):394–399. doi:10.1016/j.jip.2010.12.009
37. Tihelka E, Cai C, Giacomelli M, et al. The evolution of insect biodiversity. *Curr Biol*. 2021;**31**(19):R1299–R1311. doi:10.1016/j.cub.2021.08.057
38. Tijssen P, Pénzes JJ, Yu Q, et al. Diversity of small, single-stranded DNA viruses of invertebrates and their chaotic evolutionary past. *J Invertebr Pathol*. 2016;**140**:83–96. doi:10.1016/j.jip.2016.09.005
39. Tokarev YS, Malysh SM, Volodartseva YV, et al. Molecular identification of a densovirus in healthy and diseased Zophobas morio (Coleoptera, Tenebrionidae). *Intervirology*. 2019;**62**(5–6):222–226. doi:10.1159/000508839
40. Tsochatzis ED, Berggreen IE, Vidal NP, et al. Cellular lipids and protein alteration during biodegradation of expanded polystyrene by mealworm larvae under different feeding conditions. *Chemosphere*. 2022;**300**:134420. doi:10.1016/j.chemosphere.2022.134420
41. van Broekhoven S, Oonincx DG, van Huis A, et al. Growth performance and feed conversion efficiency of three edible mealworm species (Coleoptera: Tenebrionidae) on diets composed of organic by-products. *J Insect Physiol*. 2015;**73**:1–10. doi:10.1016/j.jinsphys.2014.12.005
42. van Griethuijsen LI, Trimmer BA. Locomotion in caterpillars. *Biol Rev Camb Philos Soc*. 2014;**89**(3):656–670. doi:10.1111/brv.12073
43. Virus taxonomy: 2021 release. International Committee on Taxonomy of Viruses (ICTV). Accessed July 2022. https://talk.ictvonline.org/taxonomy/.
44. Weihmann T, Kleinteich T, Gorb S, et al. Functional morphology of the mandibular apparatus in the cockroach Periplaneta americana (Blattodea: Blattidae)—a model species for omnivore insects. *Arthropod Syst Phylogeny*. 2015;**73**:477–488.
45. Yang Y, Yang J, Wu WM, et al. Biodegradation and mineralization of polystyrene by plastic-eating mealworms: part 1. Chemical and physical characterization and isotopic tests. *Environ Sci Technol*. 2015;**49**(20):12080–12086. doi:10.1021/acs.est.5b02661